Research Square

Preprints are preliminary reports that have not undergone peer review.
They should not be considered conclusive, used to inform clinical practice,
or referenced by the media as validated information.

An integrative network medicine approach identifies Erlotinib as a repurposed therapeutic candidate for obesity

Kun Liu
Hunan Normal University
Lei Xiong
Hunan Normal University
Yu-kai Ge
Hunan Normal University
Xue Yu
Hunan Normal University
Ling Liu
Hunan Normal University
Jin-Rui Lv
Hunan Normal University
Shen-Shu Yang
Hunan Normal University
Chun-Hong Dong
Henan University of Chinese Medicine
Hua-Ping Xie
hpxie@hunnu.edu.cn

Hunan Normal University

Research Article

Keywords: Obesity, drug repositioning, Erlotinib, BMP2K

Posted Date: August 26th, 2026

DOI: https://doi.org/10.21203/rs.3.rs-10469287/v1

License: This work is licensed under a Creative Commons Attribution 4.0 International License.
Read Full License

Abstract

Background

Obesity is a complex metabolic disorder characterized by adipose tissue dysfunction, chronic inflammation, and lipid metabolism disorders. Current anti-obesity therapies remain limited by efficacy and safety concerns. Drug repurposing offers an efficient strategy for therapeutic discovery, but cell-type-specific approaches are still lacking.

Methods

We developed a cell-type-specific drug repositioning framework by integrating human adipose tissue single-cell RNA sequencing, obesity GWAS, hdWGCNA, transcription factor regulatory analysis, network medicine, machine learning, molecular docking analysis, molecular dynamics simulations (MD), and in vivo validation. Obesity-associated cellular populations and therapeutic candidates were identified through multi-layer network analysis and subsequently validated in a zebrafish obesity model.

Results

Four obesity-associated pathogenic cell populations, including SAT_AC, SAT_MC, VAT_AC, and VAT_EC, were identified and exhibited distinct alterations in cellular communication, transcriptional regulation, and metabolic functions. Network-based drug repositioning analysis prioritized Erlotinib, a clinically approved epidermal growth factor receptor (EGFR) tyrosine kinase inhibitor, as a potential therapeutic candidate for obesity. MR analysis further supported causal associations between several Erlotinib-related targets and obesity. Integrated transcriptomic analysis and machine learning identified BMP2K as a potential functional target of Erlotinib, while molecular docking and MD demonstrated favorable binding affinity and stable protein–ligand interactions. In vivo validation showed that Erlotinib significantly reduced obesity-associated body weight gain, body mass index (BMI), and triglyceride accumulation. Moreover, Erlotinib modulated lipid metabolism-related genes (*fasn*, *srebf1*, and *pparab*), suppressed inflammatory cytokines (*tnfa* and *il1b*), and partially reversed obesity-associated *bmp2k* upregulation.

Conclusion

This study establishes a cell-type-specific integrative framework for obesity drug repositioning by combining single-cell transcriptomics, genetic evidence, computational prediction, and experimental validation. Our findings identify Erlotinib, an EGFR-targeted anticancer drug, as a potential therapeutic candidate for obesity and provide mechanistic insights into its metabolic effects, highlighting BMP2K as a candidate mediator of Erlotinib-associated anti-obesity activity.

Introduction

Obesity, currently defined by a BMI of 30 kg/m² or higher, has become a global epidemic[1]. Since 1975, its prevalence has surged across all age groups, with a growing number of children and adolescents now affected, and it is estimated that by 2030, over half of the elderly population will be overweight or obese[2–4]. This escalating trend translates into an enormous socioeconomic and healthcare burden worldwide[5–7].

Obesity is a complex condition that substantially elevates the risk of multiple comorbidities, including cardiovascular disease[8, 9], diabetes[10], reduced fertility[11], inflammation[12], and cancer[13]. A hallmark of obesity is chronic low-grade inflammation, primarily driven by dysfunctional white adipose tissue (WAT). WAT comprises two main depots—subcutaneous adipose tissue (SAT) and visceral adipose tissue (VAT)—with VAT being the more metabolically active compartment. VAT continuously releases pro-inflammatory cytokines and free fatty acids, directly promoting insulin resistance, type 2 diabetes, fatty liver disease and cardiovascular disorders, thus representing a central driver of obesity-related pathogenesis[14–16].

Single-cell RNA sequencing (scRNA-seq) enables high-resolution profiling of individual cells to reveal their distinct states and functions. Since its introduction, scRNA-seq has greatly facilitated the discovery of novel cell types and provided breakthrough insights into various diseases[17]. In the context of WAT, scRNA-seq studies have revealed a complex cellular ecosystem comprising adipocytes, stromal cells and immune cells, highlighting the marked heterogeneity between SAT and VAT depots[18–20].

Despite substantial efforts in obesity prevention and management, current therapeutic options remain suboptimal. Bariatric surgery effectively reduces BMI and associated disease risks, but postoperative challenges—including weight regain and long-term complications—persist[21, 22]. For patients unsuitable for or unwilling to undergo surgery, pharmacotherapy serves as an important alternative; however, available drugs are limited by insufficient efficacy, safety concerns, and restricted choices[23]. Even recently approved agents such as semaglutide, despite demonstrating substantial weight-loss efficacy, face unresolved issues including weight rebound after discontinuation, high cost, gastrointestinal side effects, and uncertain long-term safety[24, 25].

Given the high failure rates and prolonged timelines of de novo drug development[26], drug repositioning —identifying new therapeutic indications for existing approved drugs—has emerged as a time-efficient and cost-effective strategy to accelerate the availability of anti-obesity therapies[27]. Previous studies have identified several repositioned candidates with potential anti-obesity effects, including rolipram and carvedilol, which showed beneficial effects on lipid metabolism and metabolic dysfunction in obesity models[28–30]. However, conventional repositioning approaches often rely on bulk-level data that mask cell-type-specific effects. Integrating network-based analyses with scRNA-seq can overcome this limitation by enabling cell-type-resolved characterization and improving the precision of candidate identification

[31–34].

In this study, we integrated multiple scRNA-seq datasets of WAT to characterize the cellular compositions of both SAT and VAT. By analyzing genome-wide association study (GWAS) data on obesity, we further screened for obesity-associated cell types. Through high-dimensional weighted gene co-expression network analysis (hdWGCNA), pySCENIC, and differential expression analysis on key cell types, we identified critical genes to construct a disease network for drug repositioning. Additionally, Mendelian randomization (MR) was applied to investigate causal relationships between drug targets and obesity, leading to candidate repositioned drugs, whose efficacy was subsequently validated using a zebrafish obesity model.

Method

Integrated analysis of scRNA-seq datasets.

In this study, all single-cell RNA sequencing datasets of white adipose tissue were sourced from the GEO database. Based on the sample information provided in the original studies, the samples were categorized into an obese group and a control group. For subcutaneous adipose tissue, datasets were obtained from GSE295708, GSE176171, GSE281365, and a study by Radiana Ferrero et al.[35], comprising 11 control samples and 22 obese samples. For visceral adipose tissue, datasets included GSE176171, GSE129363, GSE225700, GSE136229 and GSE163830, totaling 2 control samples and 16 obese samples. Data processing followed the standard workflow of the R package Seurat, integration of multiple datasets was performed using CCAIntegration method and batch effects across samples were mitigated using the Harmony package[36]. Cell annotation was performed based on marker genes for distinct cell types identified through literature review.

Identifying disease-associated cell types

The identification of disease-related cell types was conducted using the single-cell disease relevance score (scDRS) method to investigate associations between specific cell populations and obesity[37]. First, gene sets linked to obesity were derived from genome-wide association studies (GWAS) summary statistics using the MAGMA tool[38]. Subsequently, scDRS was employed to evaluate the disease relevance of individual cells by quantifying the enrichment of these candidate risk genes within each cell's expression profile, with statistical significance assessed through permutation-based p-values. The obesity GWAS datasets utilized in this analysis were retrieved from the open GWAS database (https://gwas.mrcieu.ac.uk).

Cell chat analysis

This study employed the CellChat tool to systematically analyze intercellular communication in WAT, aiming to elucidate dynamic changes in signaling pathways among different cell types under obese

conditions[39].

Differential expression analysis

Differential expression analysis was performed using the FindMarkers function to identify differentially expressed genes (DEGs) between control and obese groups across distinct cell types. Genes meeting the thresholds of |avg_log2FC| > 0.25 and adjusted p-value (p_val_adj) < 0.05 were considered statistically significant.

Enrichment analysis

To investigate the biological pathways associated with DEGs and core candidate genes, we performed functional enrichment analysis based on the Gene Ontology (GO) framework. This analysis was implemented using the clusterProfiler R package[40], with GO terms considered statistically significant at a threshold of p-value < 0.05.

High-dimensional weighted gene co-expression network analysis (hdWGCNA)

The fundamental principle of co-expression network analysis is to group genes into distinct functional modules based on the similarity of their expression profiles[41]. To apply this principle to high-dimensional scRNA-seq data, we employed hdWGCNA[42]. This method represents an extension and refinement of the classic WGCNA framework, specifically designed to construct robust co-expression networks and identify disease-associated modules from scRNA-seq datasets.

Single-cell regulatory network inference and clustering (SCENIC) analysis

SCENIC is a computational method specifically designed for inferring transcription factor (TF) activity from scRNA-seq data[43]. Its core functionality is to decipher the regulatory relationships between TF and their downstream target genes within scRNA-seq datasets. This analysis reveals the regulatory state of individual cells and the biological properties of cell populations, thereby aiding in the inference of cell states and functions. In this study, we performed the SCENIC analysis using the pySCENIC implementation.

Drug repositioning analysis

A network-based strategy was employed for drug repositioning analysis in this study[33]. In brief, known drug targets were mapped onto the human proteome and subsequently linked to disease modules.

Specifically, key genes identified from obesity-associated cell types via scDRS analysis were extracted to construct a disease-specific network. Using established drug–target interaction data provided by the original reference, a drug–target network was built. The network proximity between drug targets and the disease module was then calculated, where a higher degree of network closeness (indicated by a lower Z-score) reflects a stronger functional association within the network.

Mendelian randomization (MR) analysis

In this analysis, genetic variants (single nucleotide polymorphisms, SNPs) associated with drug targets were selected as instrumental variables from the GTEx database (https://gtexportal.org/home). Outcome data were retrieved from publicly available GWAS on obesity in the openGWAS database. Instrumental SNPs were filtered based on a genome-wide significance threshold ($p < 5\times10^{-8}$) and a linkage disequilibrium threshold ($r^2 < 0.1$) to ensure their independence and relevance.

The primary causal estimates were derived using the inverse-variance weighted (IVW) method. Heterogeneity among SNP effects was assessed via Cochran's Q test, and potential pleiotropic bias was evaluated using the MR-Egger intercept test. Finally, a leave-one-out sensitivity analysis was performed by iteratively excluding individual SNPs to verify the robustness of the MR results.

Potential target prediction of erlotinib

To establish a theoretical basis for drug repositioning, this study explored the polypharmacology of Erlotinib using online computational platforms. The SMILES notation of Erlotinib was retrieved from PubChem, and potential targets were predicted via SwissTargetPrediction (https://www.swisstargetprediction.ch/) and SEA search server (https://sea.bkslab.org/jobs/search_a4ac9f72-22c9-45df-bd9f-0c67a4183078).

Differential gene expression analysis

Subcutaneous adipose tissue transcriptomic datasets GSE152991 and GSE205741 were obtained from the Gene Expression Omnibus (GEO) database. Differential gene expression analysis of the bulk RNA-sequencing data was performed using the DESeq2 package in R. Genes with an adjusted p-value < 0.05 and an absolute log2 fold change ($|\log2FC| \geq 1$ were considered DEGs.

Machine learning-based screening and diagnostic evaluation of candidate genes for obesity

To screen candidate genes for the diagnosis of obesity, we performed LASSO and random forest (RF) analyses. The overlapping genes identified by both machine learning methods were considered candidate hub genes. Subsequently, a nomogram was constructed using the "rms" package to evaluate the diagnostic value of these genes, and receiver operating characteristic (ROC) curve analysis was

performed to assess diagnostic efficacy. An area under the curve (AUC) greater than 0.7 was considered indicative of good diagnostic accuracy.

Molecular docking analysis

To gain deeper insights into how Erlotinib interacts with the chosen target proteins, molecular docking simulations were carried out. The structures of the ALK (PDB: 3AOX) and BMP2K (PDB:4W9W)-were retrieved from the Protein Data Bank (https://www.rcsb.org/). The AutoDock Vina software was utilized for docking computations, aiming to evaluate the binding affinity as well as the intermolecular interaction patterns between Erlotinib and targets.

Molecular dynamics (MD) simulations

MD simulations were performed using GROMACS software[44]. Ligand topologies were parameterized with the AMBER force field, whereas the AMBER99SB force field was applied to the protein. The system was solvated with TIP3P water in a triclinic periodic box, neutralized by NaCl, and energy-minimized over 1000 steps via the steepest-descent method. Subsequent equilibration was carried out under NVT and NPT ensembles, followed by a 100 ns production simulation under periodic boundary conditions. A minimum distance of 1.0 nm was maintained between the protein and box edges in all directions, and a 2 fs time step was used throughout. Both Coulombic and van der Waals interactions were truncated at 1.4 nm.

Root-mean-square deviation (RMSD) measures the average conformational drift of the system relative to its starting structure and provides a principal indicator of global structural stability. In ligand–receptor docking studies, RMSD is routinely applied to assess the stability of the ligand's binding pose and the maintenance of the bound complex. Root-mean-square fluctuation (RMSF) quantifies residue- or atom-level positional variability during the simulation, revealing local flexibility and dynamic profiles along the protein chain. The Free Energy Landscape (FEL) is widely used to characterize the conformational space sampled by molecules during simulations and the associated free-energy states. By representing free-energy minima and transition barriers, FEL provides insights into the free-energy distribution of complex systems and facilitates the identification of thermodynamically stable and metastable conformational states.

In vivo experimental procedure

Wild-type TU (Tuebingen) zebrafish were obtained from the College of Life Sciences, Hunan Normal University. All zebrafish experiments were conducted in compliance with ethical guidelines approved by the Institutional Animal Care and Use Committee of Hunan Normal University. Embryos and juvenile zebrafish were maintained under stable environmental conditions, including a temperature of 28.5°C and a 14-hour light/10-hour dark photoperiod. Fish were fed twice daily according to established laboratory zebrafish husbandry protocols.

Three-month-old zebrafish were randomly assigned into six groups (n = 20 per group) and housed in a 1 L culture system under the following feeding regimens: Group A (Control): normal diet. Group B (Obese):

high-fat diet to induce overfeeding. Group C and D (Obese + Erlotinib): high-fat diet + erlotinib treatment at concentrations of 500 mg/kg and 1000 mg/kg, respectively. Groups E (Obese + Orlistat): high-fat diet + orlistat treatment (500 mg/kg, positive control). All treatment groups (B–E) followed the same high-fat feeding protocol as Group B. Administer an intraperitoneal injection every other day. Body weight and length were measured once every three days. Body mass index (BMI) values were calculated using the following formula: body weight (g)/body length^2 (cm^2). On day 21, zebrafish from each group were sacrificed, and serum samples were collected for triglyceride measurement.

Analysis of relative gene expression of inflammatory markers

From zebrafish liver tissue, total RNA was extracted and quantified. The expression levels of mRNA were determined by qRT-PCR, with β-actin used as the internal control gene. Primer sequences are listed in Table 1.

Table 1
The sequences of primers for RT-qPCR used in this study

Name	Primers for PCR (5'-3')	Product length
fasn	qF1: GAGAAAGCTTGCCAAACAGG	203
	qR1: GAGGGTCTTGCAGGAGACAG	
srebf1	qF1: CATCCACATGGCTCTGAGTG	250
	qR1: CTCATCCACAAAGAAGCGGT	
pparab	qF1:GCTGGACGATAGTGACCTCG	88
	qR1: CTCGATATGCGGGACGTTCA	
tnfa	qF1:GGAGAGTTGCCTTTACCGCT	145
	qR1: CCTGGGTCTTATGGAGCGTG	
il1b	qF1:GGATCTCCACATTTGCAGGC	190
	qR1: GTACGAGATGTGGAGCGGAG	
bmp2k	qF1: CCAGTGTCTGCTGTGGATGT	171
	qR1: TGATCGCTCCACTGGCTTTT	

Statistical analysis

Statistical analyses were performed using GraphPad Prism software. Differences among multiple groups were assessed by one-way ANOVA, followed by the Tukey post hoc test for pairwise comparisons. A p-value < 0.05 was considered statistically significant. All data are presented as mean ± standard deviation (SD).

Result

The cell communication of obesity-associated cell types.

To systematically characterize key cellular populations associated with obesity, we first integrated multiple single-cell datasets from SAT and VAT (Fig. 1A). Cellular annotation of the scRNA-seq data from different tissues was performed based on previously reported marker genes and those provided by the CellMarker database. A total of 11 distinct cell types were annotated in the single-cell data derived from SAT (Fig. 1B). To identify cell types linked to obesity, we performed an integrated analysis of scRNA-seq data and GWAS data using the scDRS method. The UMAP visualization revealed that cell types significantly associated with obesity included AC, ASC, EC, LC, MastC, Mural and B cells (Fig. 1C). Analysis of the VAT single-cell data led to the annotation of 8 cell types (Fig. 1D), among which AC, APC, EC, LC, and SMC showed significant associations with obesity (Fig. 1E). Detailed results of the scDRS analysis are summarized in Table 2.

Table 2
Associations of cell populations from different tissues for obesity.

SAT					
group	n_cell	assoc_mcp	assoc_mcz	hetero_mcp	hetero_mcz
AC	42061	0.001	10.041	0.001	15.583
ASC	31347	0.001	12.608	0.001	21.145
EC	14550	0.001	11.323	0.001	15.778
LC	1034	0.001	39.676	0.001	11.327
MastC	2727	0.001	5.719	0.001	13.481
Mural	4742	0.001	14.908	0.001	15.297
B	781	0.003	3.034	0.004	3.664
MC	35352	0.677	-0.427	0.001	10.971
T	9537	0.820	-0.939	0.001	16.815
APC	8444	1.000	-10.369	0.001	10.282
SMC	592	1.000	-6.191	0.001	6.719
VAT					
group	n_cell	assoc_mcp	assoc_mcz	hetero_mcp	hetero_mcz
AC	15884	0.001	8.027	0.001	20.862
APC	50494	0.001	28.132	0.001	23.491
EC	7177	0.001	15.629	0.001	23.327
LC	2222	0.001	17.725	0.001	16.638
SMC	2304	0.001	19.954	0.001	17.552
MC	12797	0.081	1.483	0.001	15.712
NK	5638	0.171	0.951	0.001	13.075
MesoC	11934	1.000	-3.249	0.001	9.550
assoc_mcp: Monte Carlo (MC) p-value for cell group-disease association.					
assoc_mcz: MC z-score for cell group-disease association.					
hetero_mcp: MC p-value for within-cell group heterogeneity in association with disease.					
hetero_mcz: MC z-score for within-cell group heterogeneity in association with disease.					

To explore the communication exchanges between control and obesity, we analyzed the intercellular communication network using the CellChat package and compared the strength of interactions between different cell populations. For SAT, the strength of interactions from AC to MC and from MC to AC were significantly enhanced in the obese group compared to the control group (Fig. 1F). Figure 1G primarily illustrated that in the obese group, cellular communication from AC to MC was mediated through SEMA3C-PLXND1, IL6-CD4, FGF1-FGFR1, ANXA1-FPR1, ANGPTL4-SDC2 and ADIPOQ-ADIPOR2 ligand-receptor pairs. The cellular communication from MC to AC was mediated through SEMA3C-(NRP1 + PLXNA2), SEMA3C-(NRP1 + PLXNA4), SEMA3C-(NRP2 + PLXNA2), SEMA3C-(NRP2 + PLXNA4), WNT2B-(FZD4 + LRP5) and WNT2B-(FZD4 + LRP6) ligand-receptor pairs. For SAT, the strength of interactions from EC to AC was significantly enhanced in the obese group (Fig. 1I), cellular communication from EC to AC was mediated through SEMA3C-(NRP1 + PLXNA4) and SEMA3C-(NRP2 + PLXNA4) ligand-receptor pairs (Fig. 1J). The cell types of our subsequent focus are AC and MC in SAT, as well as AC and EC in VAT.

Enrichment analysis of DEGs and TFs in key cell types

To investigate the functions of DEGs in key cell types between the control and obese groups, we conducted differential analysis on the two groups. The heatmap in Fig. 2A illustrated the top five up- and down-regulated genes in the obese group. To further characterize the functional profiles of these four cell types, GO (Fig. 2B) and KEGG (Fig. 2C) functional enrichment analyses were performed. GO enrichment analysis revealed that DEGs in SAT_AC were primarily enriched in lipid metabolism-related signaling pathways, such as “fatty acid oxidation” and “regulation of lipid metabolic process”. In SAT_MC, in addition to pathways related to inflammation such as regulation of inflammatory response, DEGs were also involved in regulating lipid metabolic pathways including “lipid storage” and “cholesterol storage”. This result indirectly supports the finding of enhanced cellular communication between MC and AC in the obese group. DEGs in VAT_AC were also enriched in lipid metabolism pathways such as “lipid storage” and “regulation of lipid metabolic process”, and additionally showed significant enrichment in the “endothelial cell migration” pathway. DEGs in VAT_EC were involved in the “regulation of angiogenesis” and “cholesterol storage”, which, together with the observed increase in EC-AC communication strength in the obese group, provides further supporting evidence.

KEGG pathway analysis revealed both shared and cell-type-specific pathway engagements. Consistent with the GO enrichment results, DEGs in both SAT_AC and SAT_MC were significantly enriched in lipid metabolism-related signaling pathways. Furthermore, DEGs in SAT_MC, VAT_AC, and VAT_EC commonly participated in regulating the “PI3K-Akt pathway”, “MAPK pathway” and “insulin resistance”.

TF analysis provided insights into the heterogeneous gene regulatory networks underlying cellular heterogeneity. Therefore, we performed TFs analysis on the key cell types using pyscenic. We displayed the enriched TFs for SAT_AC (Fig. 2D), SAT_MC (Fig. 2E), VAT_AC (Fig. 2F), and VAT_EC (Fig. 2G) in

different groups. Sup Table 1–4 list the TFs with significantly altered activity between the control and obese groups, along with their predicted target genes.

Screening of obese-related co-expression network modules in different cell types

HdWGCNA was employed to identify obesity-associated co-expression modules across distinct cell types. The optimal soft-thresholding power for each cell type was determined using the GetPowerTable function. For the construction of obesity-related co-expression networks in SAT_AC, SAT_MC, VAT_AC and VAT_EC, the selected soft-thresholding powers were 8, 6, 7 and 7, respectively.

In SAT_AC, the hierarchical clustering dendrogram (Fig. 3A) revealed 14 distinct co-expression modules, designated AC-M1 through AC-M14. Among these, modules AC-M2, AC-M7, AC-M5, AC-M12, AC-M14, AC-M6, AC-M1 and AC-M10 showed a significant positive correlation with obesity and are highlighted in red in Fig. 3B. We further examined inter-module relationships: in the correlation matrix (Fig. 3C), a stronger positive correlation between two modules is indicated by a color closer to purple and a larger tile area.

Similarly, dendrograms in Figs. 3D, 3G and 3J display the co-expression modules identified in the SAT_MC, VAT_AC and VAT_EC networks, respectively. Dot plots in Figs. 3E, 3H and 3K illustrate the modules that are significantly associated with obesity in each corresponding network. Module–module correlation matrices for the SAT_MC, VAT_AC and VAT_EC networks are presented in Figs. 3F, 3I and 3L, respectively.

Drug repositioning analysis

To identify key genes associated with obesity, we performed an intersection analysis using DEGs from four cell types (SAT_AC, SAT_MC, VAT_AC and VAT_EC) in obese and control groups, along with genes from hdWGCNA-derived modules that showed significant positive correlation with obesity, as well as downstream target genes of TFs enriched in the obese group. This process yielded key gene sets for each cell type. Subsequently, we constructed cell-type-specific obese disease networks based on the intersection genes obtained from SAT_AC (Fig. 4A), SAT_MC (Fig. 4B), VAT_AC (Fig. 4C) and VAT_EC (Fig. 4D), and performed drug repurposing analysis using a network proximity-based approach. Ultimately, based on the screening criteria of $Z < -2$ and $P < 0.05$, six candidate drugs identified across all four cell types were selected (Fig. 4E), with their corresponding DrugBank IDs highlighted in bold red in Fig. 4F.

After obtaining the targets of the drugs from DrugBank database, we used MR analysis to evaluate the causal relationship between the drug targets and obesity, and Table 3 shows the list of targets used for MR. The IVW results revealed significant causal associations between the gene expression of drug

targets NR1I2 (OR = 0.656, 95% CI = 0.449–0.959, *P* = 0.029), PDGFRB (OR = 0.760, 95% CI = 0.580–0.995, *P* = 0.046), KDR (OR = 0.869, 95% CI = 0.778–0.971, *P* = 0.013), FGFR2 (OR = 1.001, 95% CI = 1.000-1.002, *P* = 0.034), FGFR1 (OR = 1.235, 95% CI = 1.066–1.431, *P* = 0.005), and SRC (OR = 1.441, 95% CI = 1.012–2.052, *P* = 0.043) with obesity (Fig. 4G).

Table 3
Target information for each drug

DrugBank ID	Drug name	Target	Actions
DB04849	Cediranib	KDR	Inhibitor
DB09063	Ceritinib	ALK	Antagonist
DB08865	Crizotinib	ALK	Inhibitor
DB01254	Dasatinib	SRC	Inhibitor
DB00530	Erlotinib	NR1I2	Agonist
DB09079	Nintedanib	FGFR1, FGFR2, SRC, PDGFRB	Inhibitor

Results of Cochran's Q test and MR-Egger intercept analysis indicated no significant heterogeneity or horizontal pleiotropy in the MR analysis (Table 4). To evaluate whether the findings were driven by individual SNPs, a leave-one-out sensitivity analysis was performed (Sup Fig. 1). The causal effects of NR1I2, PDGFRB, KDR, FGFR2, FGFR1, and SRC on obesity remained consistent after systematically excluding each SNP, supporting the robustness of the observed causal relationships.

Table 4
The results of Cochran's Q test and MR-Egger intercept analysis in the MR analysis.

exposure	Cochran's Q test				MR-Egger intercept analysis		
	method	Q	Q_df	Q_pval	egger_intercept	se	pval
NR1I2	MR Egger	2.540	3	0.468	-0.165	0.192	0.479
	IVW	2.520	2	0.284			
PDGFRB	MR Egger	2.540	3	0.317	0.131	0.099	0.315
	IVW	2.520	2	0.414			
KDR	MR Egger	2.121	3	0.548	0.015	0.037	0.722
	IVW	1.953	2	0.377			
FGFR2	MR Egger	4.785	3	0.188	0.000	0.001	0.818
	IVW	4.626	2	0.099			
FGFR1	MR Egger	4.217	3	0.239	0.109	0.093	0.363
	IVW	2.504	2	0.286			
SRC	MR Egger	2.847	3	0.416	0.201	0.323	0.597
	IVW	2.384	2	0.304			

Based on MR analysis, KDR and PDGFRB – as the inhibitor for Cediranib (DB04849) and Nintedanib (DB09079), respectively - were identified as protective factors against obesity, suggesting that Cediranib and Nintedanib may potentially promote weight gain. However, FGFR1, FGFR2 and SRC are also inhibited by Nintedanib. Notably, SRC - a target of Dasatinib (DB01254) - was found to be a risk factor for obesity in MR analysis, implying that Dasatinib may possess anti-obesity effects, which is supported by existing reports[45, 46]. Furthermore, combined administration of Nintedanib and Celecoxib has been shown to improve systemic metabolism in obese mice[47]. Given these conflicting lines of evidence and the complex multi-target profile of these compounds, Cediranib and Nintedanib will not be the primary focus of this study. In contrast, NR1I2 - an agonist for Erlotinib (DB00530) - emerged as a protective factor against obesity in the MR analysis, indicating that erlotinib may have the potential to suppress obesity. Moreover, the role of Erlotinib in obesity remains largely unexplored. Therefore, this study will focus on investigating the functional effects of Erlotinib in the context of obesity.

Identification and validation of potential Erlotinib targets in obesity

To further identify the potential targets of Erlotinib, differential expression analysis was first performed on the GSE152991 dataset to identify DEGs between the obesity and control groups (Fig. 5A).

Subsequently, the DEGs were intersected with the predicted targets of Erlotinib obtained from the SEA and SwissTargetPrediction databases, resulting in the identification of 17 overlapping candidate genes (Fig. 5B).

Next, machine learning approaches were employed to identify core targets. Based on LASSO regression analysis, 6 feature genes were identified as potential key therapeutic targets (Fig. 5C). To further evaluate their diagnostic value for obesity, logistic regression analysis was performed, and ROC curve analysis demonstrated that all six candidate target genes exhibited good diagnostic performance, as indicated by their AUC values (Fig. 5D).

To further validate the reliability of these findings, an independent GEO dataset (GSE205741) was used for further validation. The results showed that ALK and BMP2K retained good diagnostic performance in the validation dataset (Fig. 5E).

To further assess the interactions between Erlotinib and the identified potential targets, molecular docking analysis was performed to evaluate the binding characteristics of Erlotinib with ALK and BMP2K. The docking results showed that the binding energy between Erlotinib and ALK was − 7.6 kcal/mol (Fig. 5F, G), whereas Erlotinib exhibited a stronger binding affinity toward BMP2K, with a binding energy of − 8.5 kcal/mol (Fig. 5H, I).

Therefore, BMP2K, which demonstrated a relatively higher binding affinity, was selected for subsequent MD simulations to further evaluate the stability of the protein–ligand interaction. The MD simulation results showed that the RMSD values remained within approximately 0.1 nm throughout the simulation period (Fig. 5J), suggesting an overall stable conformation of the protein–ligand complex. Furthermore, RMSF analysis identified regions with relatively high residue flexibility, reflecting local conformational fluctuations within the protein structure (Fig. 5K).

In addition, FEL analysis revealed a distinct and concentrated low-energy region in the conformational space. This region was characterized by a single and continuous energy basin, suggesting that the system predominantly remained in a dominant conformational state with a relatively focused conformational distribution during the simulation (Fig. 5L). Furthermore, the three-dimensional FEL plot provided a more intuitive visualization of this deep energy basin, further supporting the existence of a relatively stable low-energy conformational state in the simulated system (Fig. 5M).

In vivo validation of the anti-obesity effects of Erlotinib in zebrafish

To evaluate the potential anti-obesity effects of Erlotinib, an obesity model was established in zebrafish followed by drug treatment. The overall morphology of male and female zebrafish in each group is presented in Fig. 6A.

Body weight and body length were measured to assess obesity-related phenotypes. Compared with the obesity group, Erlotinib treatment significantly attenuated obesity-induced body weight gain in zebrafish (Fig. 6B). No significant differences in body length were observed among the groups (Fig. 6C). However, Erlotinib treatment significantly reduced BMI in obese zebrafish (Fig. 6D).

In the zebrafish obesity model, the mRNA expression level of the target gene *bmp2k* was significantly increased. Erlotinib treatment partially reversed the upregulation of *bmp2k* to varying degrees, whereas the positive control group did not exhibit an apparent reversal effect on *bmp2k* expression (Fig. 6E), suggesting that *bmp2k* may be regulated by Erlotinib.

Further analysis of lipid metabolism–related genes showed that the obesity-associated genes *fasn* and *srebf1* were significantly upregulated in the obesity group, whereas the expression of the obesity-protective gene *pparab* was significantly reduced. Erlotinib treatment significantly suppressed the expression of *fasn* (Fig. 6F) and *srebf1* (Fig. 6G), while promoting *pparab* expression (Fig. 6H).

In addition, Erlotinib treatment markedly attenuated the obesity-induced upregulation of inflammatory cytokines, including *tnfa* (Fig. 6I) and *il1b* (Fig. 6J). qRT-PCR results indicated that Erlotinib could regulate the abnormal expression of lipid metabolism–related genes and inflammatory factors at the molecular level in the obesity model. Finally, TG levels were measured in each group. The obesity-associated increase in serum TG levels was markedly suppressed following Erlotinib treatment (Fig. 6K).

Discussion

Through integrative multi-omics analysis, this study identified cell types associated with obesity in distinct white adipose tissues and established a systematic drug repositioning framework, nominating Erlotinib as a potential candidate for obesity intervention. In vivo zebrafish experiment results demonstrated that Erlotinib not only suppresses BMI in overfed zebrafish but also modulates lipid metabolism and inhibits inflammatory responses.

Obesity is a heterogeneous metabolic disorder whose pathological processes in SAT and VAT are driven by distinct cellular mechanisms[6]. The dysregulation of adipocytes, immune cells, and stromal cells in both SAT and VAT depots collectively constitutes the cellular basis of obesity and its related complications[19]. ScRNA-seq technology can accurately identify complex cell types in highly heterogeneous lesion tissues[48]. Although existing literature has characterized cell types in SAT and VAT[18], we integrated single-cell transcriptomic datasets from multiple sources to construct a more comprehensive and cross-dataset cellular atlas of adipose tissues across different depots. This comprehensive atlas, when integrated with GWAS data, enables systematic dissection of the functional and interactomic heterogeneity within obesity-relevant cell clusters. By further combining this atlas with GWAS data, we identified obesity-associated cell populations. This integrated approach enables a more systematic dissection of the functional and interactomic heterogeneity within obesity-relevant cell clusters, providing a novel data foundation for deeper insights into the pathological remodeling mechanisms of adipose tissue.

Current therapeutic strategies for obesity primarily aim to control body weight or improve metabolic parameters, yet they often struggle to achieve sustained long-term efficacy or reverse pathological progression. Recent advances in network medicine have created new opportunities for the repositioning of existing drugs[49]. Integrative approaches combining single-cell and GWAS data enable precise identification of key cell types critically involved in the development and progression of obesity (SAT_AC, SAT_MC, VAT_AC, VAT_EC). Focusing drug repositioning efforts on these core pathological cell types, rather than on broad tissue or organ-level analyses, holds promise for substantially enhancing the targeting, efficacy, and long-term sustainability of therapeutic strategies.

Erlotinib has been identified as a high-confidence candidate for drug repurposing in obesity. This conclusion is based on network-proximity analysis between obesity-related disease modules and drug-target networks, combined with MR analysis of relevant targets. As a well-characterized EGFR tyrosine-kinase inhibitor, Erlotinib has been used in clinical oncology for nearly two decades, with a clearly documented safety profile that includes known adverse effects such as skin rash, diarrhea, and rare hepatotoxicity[50]. Within its established therapeutic dose range (100–150 mg/day), the incidence of serious adverse events is low, and unlike certain metabolic interventions, Erlotinib carries no risk of hypoglycemia or cardiovascular stress[51].

Importantly, EGFR signaling has been closely linked to adipogenesis and adipose tissue remodeling. In both SAT and VAT, EGFR mRNA levels are positively correlated with key adipogenic genes, including ADIPOQ, SLC2A4, FSP27, PLIN1 and PPARG. In vitro experiment results demonstrate that knockdown of EGFR in human preadipocytes and mature adipocytes significantly downregulates the expression of these adipogenesis-related genes[52]. Moreover, specific activation of EGFR in adipose-tissue macrophages (ATMs) serves as a critical driver of obesity-related metabolic dysregulation; inhibiting EGFR concurrently reduces ATM accumulation, ameliorates adipose tissue inflammation and fibrosis, and enhances insulin sensitivity[53].

These mechanistic insights position erlotinib as a promising multi-faceted agent for obesity intervention: by inhibiting EGFR, it may simultaneously suppress adipogenesis in fat-storing cells and attenuate macrophage-driven inflammation in adipose tissue, thereby addressing both lipid-accumulation and chronic low-grade inflammation – two hallmarks of obesity pathogenesis. Given its well-established clinical safety and the growing evidence linking EGFR to adipose biology, Erlotinib warrants further preclinical and clinical evaluation as a repurposed therapy for obesity and its metabolic complications.

The therapeutic efficacy of Erlotinib was demonstrated in the zebrafish obesity model, as evidenced by the attenuation of obesity-associated phenotypes and the improvement of metabolic abnormalities. Erlotinib treatment significantly reduced body weight gain, BMI, and TG accumulation without affecting body length, suggesting that its beneficial effects were primarily associated with metabolic regulation rather than general growth inhibition. In addition, Erlotinib effectively modulated the expression of genes involved in lipid metabolism and inflammation, including the downregulation of *fasn*, *srebf1*, *tnfa* and *il1b*, along with the upregulation of *pparab*. These findings indicate that Erlotinib may exert anti-obesity

effects through coordinated regulation of lipid synthesis, lipid utilization, and inflammatory responses. Notably, *bmp2k*, identified through integrated bioinformatics analysis and molecular simulations, showed elevated expression in the obesity model and was partially reversed following Erlotinib treatment. Combined with the favorable binding affinity and stable protein–ligand interactions observed in silico, these findings suggest that BMP2K may contribute to the therapeutic effects of Erlotinib in obesity. However, the precise molecular mechanisms underlying BMP2K-mediated regulation remain unclear and require further investigation through targeted functional experiments.

In summary, this study demonstrates that Erlotinib exerts multiple beneficial effects, including suppressing BMI, modulating lipid metabolism, and inhibiting inflammatory responses. Collectively, these findings indicate that Erlotinib is a promising therapeutic candidate for obesity intervention, with a multi-faceted mechanism of action and clear potential to modify disease progression.

Conclusion

In summary, this study establishes an analytical framework for drug repositioning in obesity through the systematic integration of single-cell RNA sequencing data from SAT and VAT. This approach facilitated the precise identification of obesity-associated pathogenic cell populations and led to the discovery of Erlotinib as a promising repurposed candidate—a conclusion strongly reinforced by genetic (MR) and experimental validation. Collectively, our findings underscore the translational potential of Erlotinib in obesity management and highlight the integrative methodology presented here as a novel, reliable paradigm to guide future drug development efforts.

Declarations

Consent for publication

All authors approve the manuscript for publication.

Data availability

All the datasets could be downloaded directly from the indicated websites.

Funding

1. This research was funded by Xiaoxiang Scholar Distinguished Professor Startup Funding for H-p X, grant number 240602.

2. This research was funded by Hunan Normal University 2026 Open Fund for Large-Scale Instrument Testing Projects grant number 26CSY236.

3. This research was funded by Hunan Normal University 2026 Open Fund for Large-Scale Instrument Testing Projects grant number 26CSY237.

Author contributions

HPX and CHD designed the study and revised the manuscript. KL contributed to the data collection and drafted the manuscript. LX provided the platform and conducted experiments with zebrafish. YKG, XY, LL, JRL and SSY provided guidance on data analysis. All authors contributed to the article and approved the submitted version.

Competing interests

The authors have no competing interests.

References

1. Shirvani-Rad S, Tabatabaei-Malazy O, Mohseni S, Hasani-Ranjbar S, Soroush AR, Hoseini-Tavassol Z, Ejtahed HS, Larijani B. Probiotics as a Complementary Therapy for Management of Obesity: A Systematic Review. Evid Based Complement Alternat Med. 2021;2021:6688450.
2. Kulaga Z, Grajda A, Gurzkowska B, Wojtylo MA, Gozdz M, Litwin MS. The prevalence of overweight and obesity among Polish school- aged children and adolescents. Przegl Epidemiol. 2016;70:641–51.
3. Collaboration NCDRF. Worldwide trends in body-mass index, underweight, overweight, and obesity from 1975 to 2016: a pooled analysis of 2416 population-based measurement studies in 128.9 million children, adolescents, and adults. Lancet. 2017;390:2627–42.
4. Kelly T, Yang W, Chen CS, Reynolds K, He J. Global burden of obesity in 2005 and projections to 2030. Int J Obes (Lond). 2008;32:1431–7.
5. Collaborators GBDO, Afshin A, Forouzanfar MH, Reitsma MB, Sur P, Estep K, Lee A, Marczak L, Mokdad AH, Moradi-Lakeh M, et al. Health Effects of Overweight and Obesity in 195 Countries over 25 Years. N Engl J Med. 2017;377:13–27.
6. Golden A. Obesity's Impact. Nurs Clin North Am. 2021;56:xiii–xiv.
7. Perdomo CM, Cohen RV, Sumithran P, Clement K, Fruhbeck G. Contemporary medical, device, and surgical therapies for obesity in adults. Lancet. 2023;401:1116–30.
8. Welsh A, Hammad M, Pina IL, Kulinski J. Obesity and cardiovascular health. Eur J Prev Cardiol. 2024;31:1026–35.
9. Ruperez C, Madeo F, de Cabo R, Kroemer G, Abdellatif M. Obesity accelerates cardiovascular ageing. Eur Heart J. 2025;46:2161–85.
10. de Tejada-Romero MJG, Saavedra-Santana P, de la Rosa-Fernandez F, Suarez-Ramirez N, Martin-Martinez A, Del Rosario FM, Sosa-Henriquez M. Effect of obesity on fragility fractures, BMD and vitamin D levels in postmenopausal women. Influence of type 2 diabetes mellitus. Acta Diabetol. 2022;59:1201–8.

11. Uddandrao VVS, Brahma Naidu P, Chandrasekaran P, Saravanan G. Pathophysiology of obesity-related infertility and its prevention and treatment by potential phytotherapeutics. Int J Obes (Lond). 2024;48:147–65.
12. Denizli M, Capitano ML, Kua KL. Maternal obesity and the impact of associated early-life inflammation on long-term health of offspring. Front Cell Infect Microbiol. 2022;12:940937.
13. Lagou MK, Karagiannis GS. Obesity-induced thymic involution and cancer risk. Semin Cancer Biol. 2023;93:3–19.
14. Norreen-Thorsen M, Struck EC, Oling S, Zwahlen M, Von Feilitzen K, Odeberg J, Lindskog C, Ponten F, Uhlen M, Dusart PJ, Butler LM. A human adipose tissue cell-type transcriptome atlas. Cell Rep. 2022;40:111046.
15. Maffeis C, Morandi A. Body composition and insulin resistance in children. Eur J Clin Nutr. 2018;72:1239–45.
16. Rasouli N, Kern PA. Adipocytokines and the metabolic complications of obesity. J Clin Endocrinol Metab. 2008;93:S64–73.
17. Tang F, Barbacioru C, Wang Y, Nordman E, Lee C, Xu N, Wang X, Bodeau J, Tuch BB, Siddiqui A, et al. mRNA-Seq whole-transcriptome analysis of a single cell. Nat Methods. 2009;6:377–82.
18. Vijay J, Gauthier MF, Biswell RL, Louiselle DA, Johnston JJ, Cheung WA, Belden B, Pramatarova A, Biertho L, Gibson M, et al. Single-cell analysis of human adipose tissue identifies depot and disease specific cell types. Nat Metab. 2020;2:97–109.
19. Reyes-Farias M, Fos-Domenech J, Serra D, Herrero L, Sanchez-Infantes D. White adipose tissue dysfunction in obesity and aging. Biochem Pharmacol. 2021;192:114723.
20. Bondareva O, Rodriguez-Aguilera JR, Oliveira F, Liao L, Rose A, Gupta A, Singh K, Geier F, Schuster J, Boeckel JN, et al. Single-cell profiling of vascular endothelial cells reveals progressive organ-specific vulnerabilities during obesity. Nat Metab. 2022;4:1591–610.
21. Carlsson LMS, Sjoholm K, Jacobson P, Andersson-Assarsson JC, Svensson PA, Taube M, Carlsson B, Peltonen M. Life Expectancy after Bariatric Surgery in the Swedish Obese Subjects Study. N Engl J Med. 2020;383:1535–43.
22. Castaneda D, Popov VB, Wander P, Thompson CC. Risk of Suicide and Self-harm Is Increased After Bariatric Surgery-a Systematic Review and Meta-analysis. Obes Surg. 2019;29:322–33.
23. Son JW, Kim S. Comprehensive Review of Current and Upcoming Anti-Obesity Drugs. Diabetes Metab J. 2020;44:802–18.
24. Chao AM, Tronieri JS, Amaro A, Wadden TA. Semaglutide for the treatment of obesity. Trends Cardiovasc Med. 2023;33:159–66.
25. Sodhi M, Rezaeianzadeh R, Kezouh A, Etminan M. Risk of Gastrointestinal Adverse Events Associated With Glucagon-Like Peptide-1 Receptor Agonists for Weight Loss. JAMA. 2023;330:1795–7.

26. Ruban A, Stoenchev K, Ashrafian H, Teare J. Current treatments for obesity. Clin Med (Lond). 2019;19:205–12.
27. Nandre RM, Terse PS. An overview of immunotoxicity in drug discovery and development. Toxicol Lett. 2025;403:66–75.
28. Pushpakom S, Iorio F, Eyers PA, Escott KJ, Hopper S, Wells A, Doig A, Guilliams T, Latimer J, McNamee C, et al. Drug repurposing: progress, challenges and recommendations. Nat Rev Drug Discov. 2019;18:41–58.
29. Doseyici S, Mehmetoglu I, Toker A, Yerlikaya FH, Erbay E. The effects of forskolin and rolipram on cAMP, cGMP and free fatty acid levels in diet induced obesity. Biotech Histochem. 2014;89:388–92.
30. Nguyen LV, Ta QV, Dang TB, Nguyen PH, Nguyen T, Pham TVH, Nguyen TH, Baker S, Le Tran T, Yang DJ, et al. Carvedilol improves glucose tolerance and insulin sensitivity in treatment of adrenergic overdrive in high fat diet-induced obesity in mice. PLoS ONE. 2019;14:e0224674.
31. Maron BA, Altucci L, Balligand JL, Baumbach J, Ferdinandy P, Filetti S, Parini P, Petrillo E, Silverman EK, Barabasi AL, et al. A global network for network medicine. NPJ Syst Biol Appl. 2020;6:29.
32. Greene CS, Voight BF. Pathway and network-based strategies to translate genetic discoveries into effective therapies. Hum Mol Genet. 2016;25:R94–8.
33. Lal JC, Mao C, Zhou Y, Gore-Panter SR, Rennison JH, Lovano BS, Castel L, Shin J, Gillinov AM, Smith JD, et al. Transcriptomics-based network medicine approach identifies metformin as a repurposable drug for atrial fibrillation. Cell Rep Med. 2022;3:100749.
34. Fiscon G, Paci P. SAveRUNNER: an R-based tool for drug repurposing. BMC Bioinformatics. 2021;22:150.
35. Ferrero R, Rainer PY, Rumpler M, Russeil J, Zachara M, Pezoldt J, van Mierlo G, Gardeux V, Saelens W, Alpern D, et al. A human omentum-specific mesothelial-like stromal population inhibits adipogenesis through IGFBP2 secretion. Cell Metab. 2024;36:1566–e15851569.
36. Korsunsky I, Millard N, Fan J, Slowikowski K, Zhang F, Wei K, Baglaenko Y, Brenner M, Loh PR, Raychaudhuri S. Fast, sensitive and accurate integration of single-cell data with Harmony. Nat Methods. 2019;16:1289–96.
37. Zhang MJ, Hou K, Dey KK, Sakaue S, Jagadeesh KA, Weinand K, Taychameekiatchai A, Rao P, Pisco AO, Zou J, et al. Polygenic enrichment distinguishes disease associations of individual cells in single-cell RNA-seq data. Nat Genet. 2022;54:1572–80.
38. de Leeuw CA, Mooij JM, Heskes T, Posthuma D. MAGMA: generalized gene-set analysis of GWAS data. PLoS Comput Biol. 2015;11:e1004219.
39. Jin S, Guerrero-Juarez CF, Zhang L, Chang I, Ramos R, Kuan CH, Myung P, Plikus MV, Nie Q. Inference and analysis of cell-cell communication using CellChat. Nat Commun. 2021;12:1088.
40. Ashburner M, Ball CA, Blake JA, Botstein D, Butler H, Cherry JM, Davis AP, Dolinski K, Dwight SS, Eppig JT, et al. Gene ontology: tool for the unification of biology. The Gene Ontology Consortium. Nat Genet. 2000;25:25–9.

41. Langfelder P, Horvath S. WGCNA: an R package for weighted correlation network analysis. BMC Bioinformatics. 2008;9:559.
42. Morabito S, Miyoshi E, Michael N, Shahin S, Martini AC, Head E, Silva J, Leavy K, Perez-Rosendahl M, Swarup V. Single-nucleus chromatin accessibility and transcriptomic characterization of Alzheimer's disease. Nat Genet. 2021;53:1143–55.
43. Aibar S, Gonzalez-Blas CB, Moerman T, Huynh-Thu VA, Imrichova H, Hulselmans G, Rambow F, Marine JC, Geurts P, Aerts J, et al. SCENIC: single-cell regulatory network inference and clustering. Nat Methods. 2017;14:1083–6.
44. Rakhshani H, Dehghanian E, Rahati A. Enhanced GROMACS: toward a better numerical simulation framework. J Mol Model. 2019;25:355.
45. Elsayed HRH, El-Gamal R, Rabei MR, Elhadidy MG, Hamed S, Othman BH, Elshaer MMA, Sedky MK, Hassan A, El-Nablaway M. Enhanced Autophagic Flux, Suppressed Apoptosis and Reduced Macrophage Infiltration by Dasatinib in Kidneys of Obese Mice. Cells 2022, 11.
46. Gu Y, Avolio E, Alvino VV, Thomas AC, Herman A, Miller PJ, Sullivan N, Faulkner A, Madeddu P. The tyrosine kinase inhibitor Dasatinib reduces cardiac steatosis and fibrosis in obese, type 2 diabetic mice. Cardiovasc Diabetol. 2023;22:214.
47. Rebiere C, Silveira AL, Oliveira A, Rouault C, Adriouch S, Dussaud S, Abatan JB, Rose C, Lecoutre S, Boissonnas A, et al. Combined pharmacological targeting of CD9(+) progenitors alleviates obesity-induced adipose tissue fibrosis and metabolic impairment. Cell Rep Med. 2025;6:102197.
48. Jovic D, Liang X, Zeng H, Lin L, Xu F, Luo Y. Single-cell RNA sequencing technologies and applications: A brief overview. Clin Transl Med. 2022;12:e694.
49. Fang J, Pieper AA, Nussinov R, Lee G, Bekris L, Leverenz JB, Cummings J, Cheng F. Harnessing endophenotypes and network medicine for Alzheimer's drug repurposing. Med Res Rev. 2020;40:2386–426.
50. Bareschino MA, Schettino C, Troiani T, Martinelli E, Morgillo F, Ciardiello F. Erlotinib in cancer treatment. Ann Oncol. 2007;18(Suppl 6):vi35–41.
51. Reck M, Mok T, Wolf J, Heigener D, Wu YL. Reviewing the safety of erlotinib in non-small cell lung cancer. Expert Opin Drug Saf. 2011;10:147–57.
52. Latorre J, Martinez C, Ortega F, Oliveras-Canellas N, Diaz-Saez F, Aragones J, Camps M, Guma A, Ricart W, Fernandez-Real JM, Moreno-Navarrete JM. The relevance of EGFR, ErbB receptors and neuregulins in human adipocytes and adipose tissue in obesity. Biomed Pharmacother. 2022;156:113972.
53. Cao S, Pan Y, Tang J, Terker AS, Arroyo Ornelas JP, Jin GN, Wang Y, Niu A, Fan X, Wang S, et al. EGFR-mediated activation of adipose tissue macrophages promotes obesity and insulin resistance. Nat Commun. 2022;13:4684.

Figures

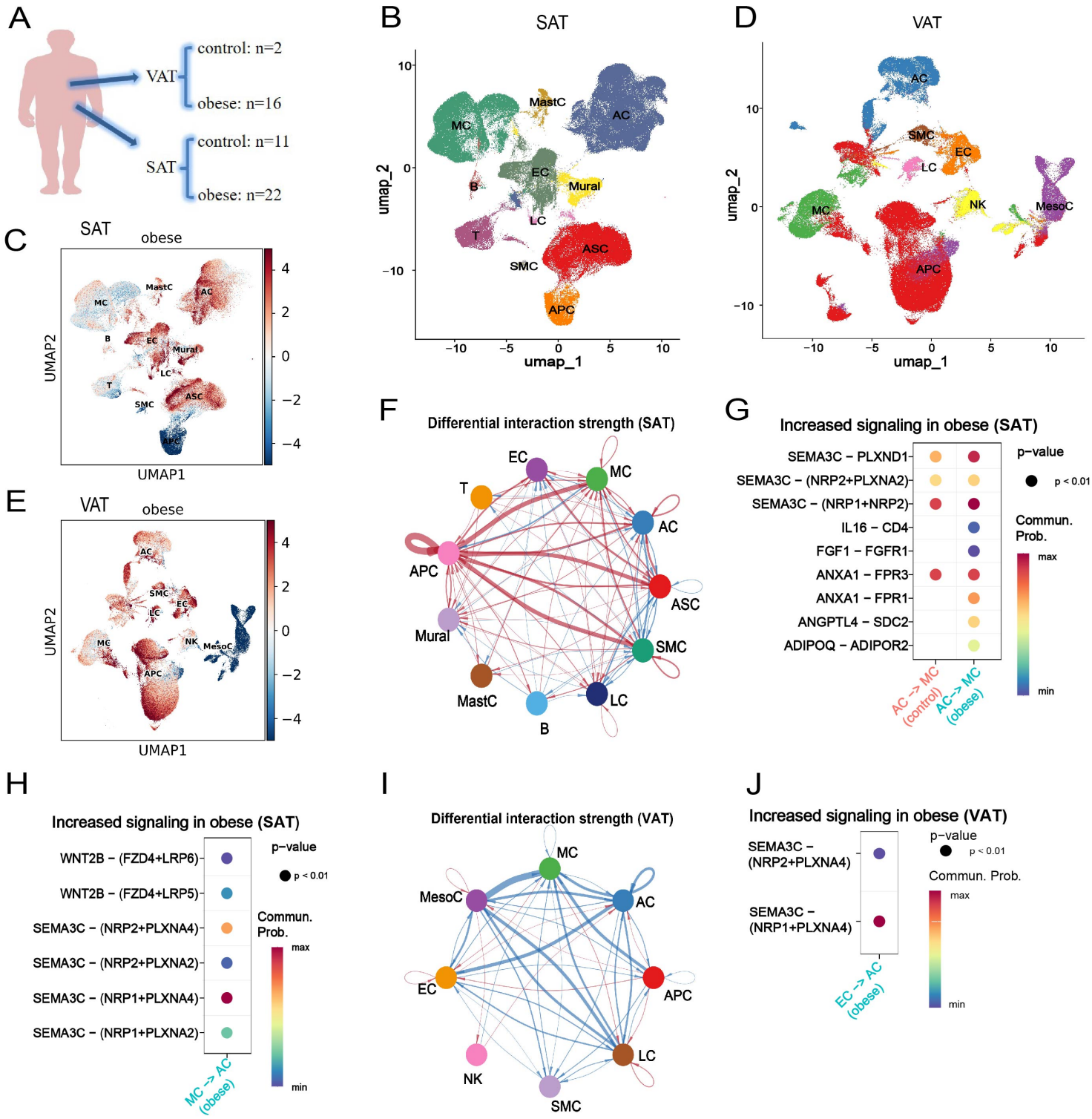


Figure 1

The cell communication of obesity-associated cell types.

Statistical analysis of scRNA-seq data from different tissues (A). Cell type annotation of single-cell RNA sequencing data from SAT (MC: macrophages, MastC: mast cell, AC: adipocytes, EC: endothelial cells, B: B cells, T: T cells, Mural: Mural cells, SMC: Smooth muscle cells, LC: Lymphatic cells, ASC: adipocyte stem cells, APC: adipocyte progenitor) (B), and identification of cell types associated with obesity (C).

Cells significantly associated with the disease are marked in red, with higher correlation values indicating stronger associations. Cell type annotation of single-cell data from VAT (AC: adipocytes, EC: endothelial cells, SMC: Smooth muscle cells, MC: macrophages, LC: Lymphatic cells, NK: Natural kill cells, MesoC: Mesothelial, APC: adipocyte progenitor) (D), and identification of cell types associated with obesity (E). Compared to the control, alterations in intercellular communication strength among distinct cell types in SAT were observed in the obese group. Red denotes enhanced communication, whereas blue indicates diminished communication (F). Ligand-receptor pair mediating SAT_AC-to-SAT_MC (G) and SAT_MC-to-SAT_AC (H) communication. Compared to the control group, alterations in intercellular communication strength among distinct cell types in VAT were observed in the obese group (I). Ligand-receptor pair mediating VAT_EC-to-VAT_AC communication (J).

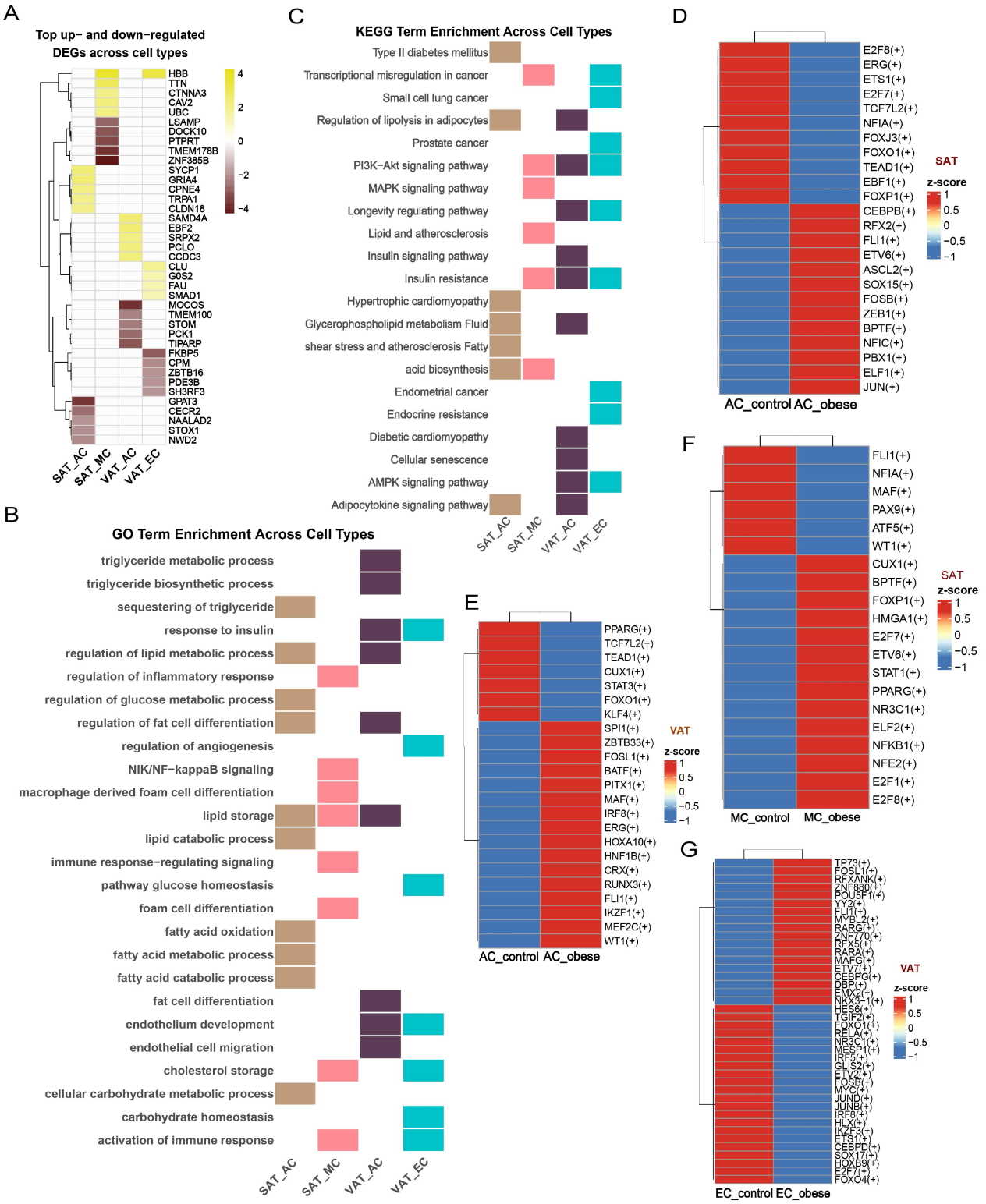


Figure 2

The functional and TF analysis of DEGs in obesity-associated cell types.

Top five most significantly upregulated and downregulated genes in the SAT_AC, SAT_MC, VAT_AC and VAT_EC (A). GO (B) and KEGG (C) enrichment analysis of DEGs for these four cell types. The enriched TFs for SAT_AC (D), SAT_MC (E), VAT_AC (F), and VAT_EC (G) in different groups.

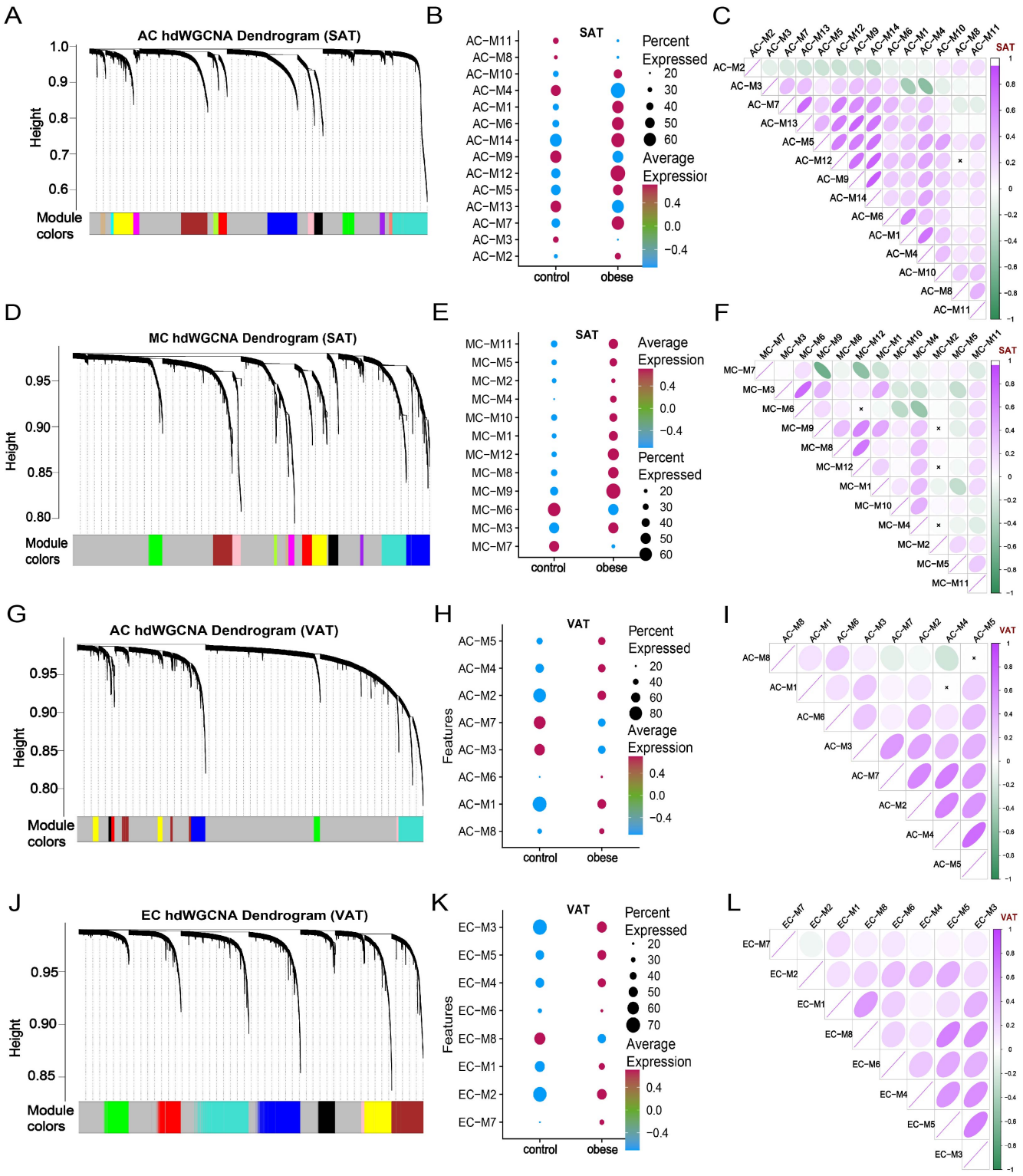


Figure 3

The results of hdWGCNA analysis.

The hierarchical clustering dendrogram for the WGCNA analysis of SAT_AC (A), SAT_MC (D), VAT_AC (G), and VAT_EC (J). The modules that significant positive correlation with obesity in SAT_AC (B), SAT_MC

(E), VAT_AC (H), and VAT_EC (K). Correlation analysis between different modules in SAT_AC (C), SAT_MC (F), VAT_AC (I), and VAT_EC (L).

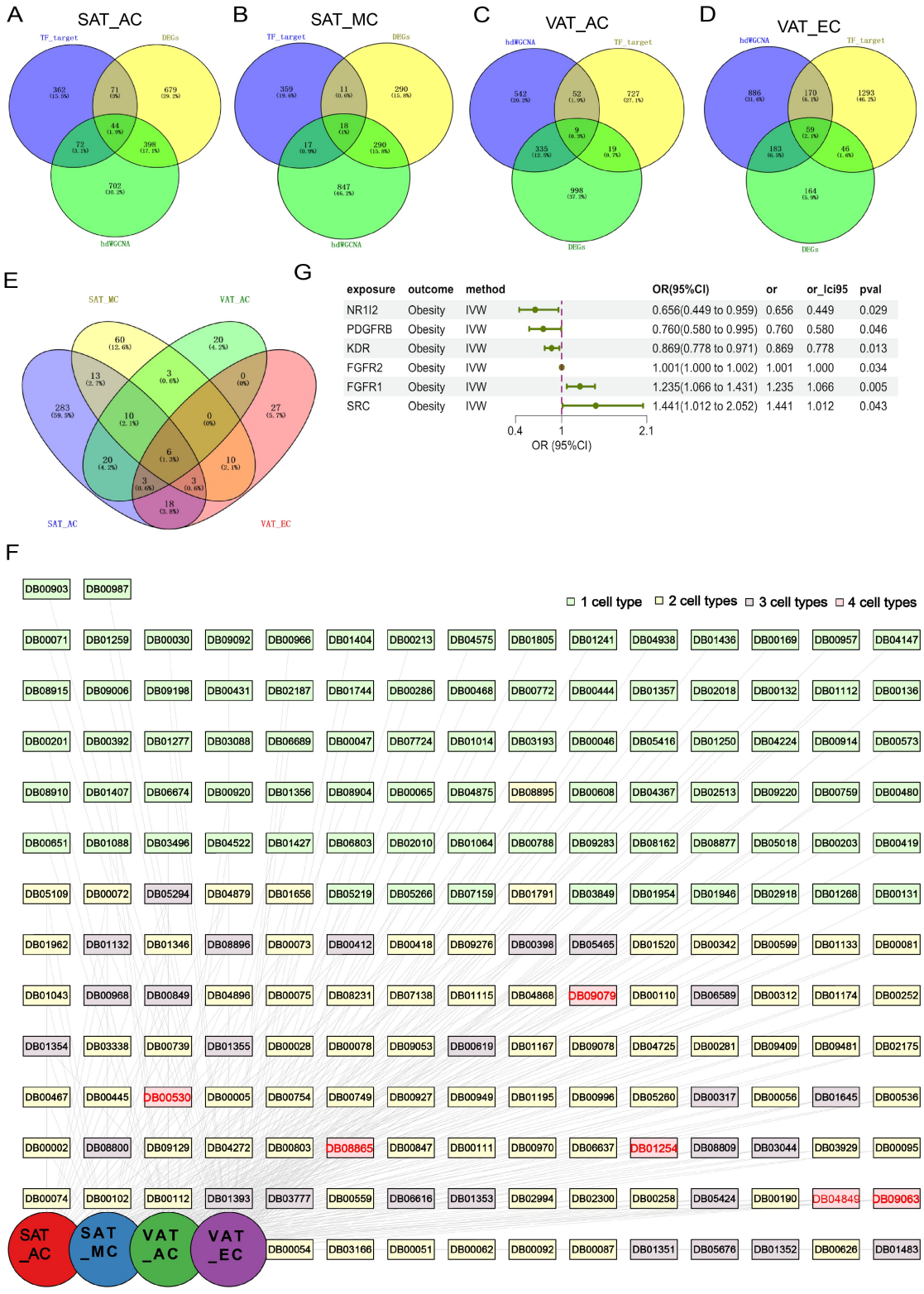


Figure 4

Drug repositioning and causal effects between the drug targets and obesity.

The intersection analysis using DEGs from SAT_AC (A), SAT_MC (B), VAT_AC (C) and VAT_EC (D) in obese and control groups, along with key genes from hdWGCNA-derived modules, as well as downstream target genes of TFs enriched in the obese group. The intersection of drugs simultaneously screened in SAT_AC SAT_MC, VAT_AC and VAT_EC (E, F). The drug targets NR1I2, PDGFRB, KDR, FGFR2, FGFR1, and SRC show significant causal relationships with obesity (G).

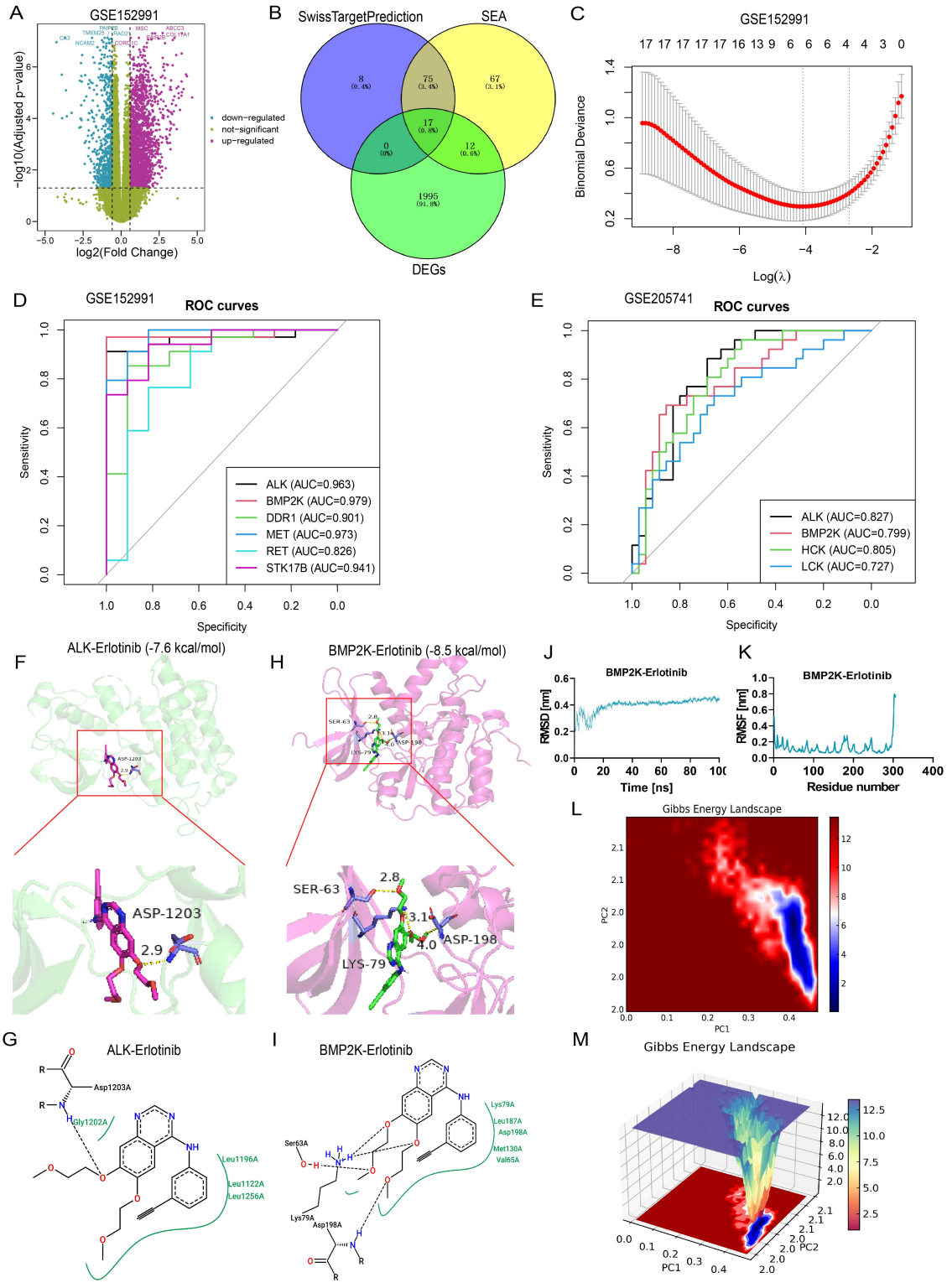


Figure 5

Identification and validation of potential Erlotinib targets in obesity.

Volcano plot showing DEGs between obesity and control groups in the GSE152991 dataset. Red and blue dots represent upregulated and downregulated genes, respectively (A). Venn diagram showing the overlap between DEGs and the predicted Erlotinib targets obtained from the SEA and SwissTargetPrediction databases (B). LASSO regression analysis for screening potential key therapeutic targets (C). ROC curves showing the diagnostic performance of the six identified candidate targets in the GSE152991 dataset (D). External validation of the diagnostic performance of ALK and BMP2K in the GSE205741 dataset (E). Molecular docking analysis showing the binding mode and interaction pattern between Erlotinib and ALK (F, G). Molecular docking analysis showing the binding mode and interaction pattern between Erlotinib and BMP2K (H, I). RMSD plot of the Erlotinib–BMP2K complex during MD simulation (J). RMSF analysis of residue flexibility in the Erlotinib–BMP2K complex (K). Two-dimensional FEL analysis of the Erlotinib–BMP2K complex (L). Three-dimensional representation of the FEL showing the dominant low-energy conformational state of the Erlotinib–BMP2K complex (M).

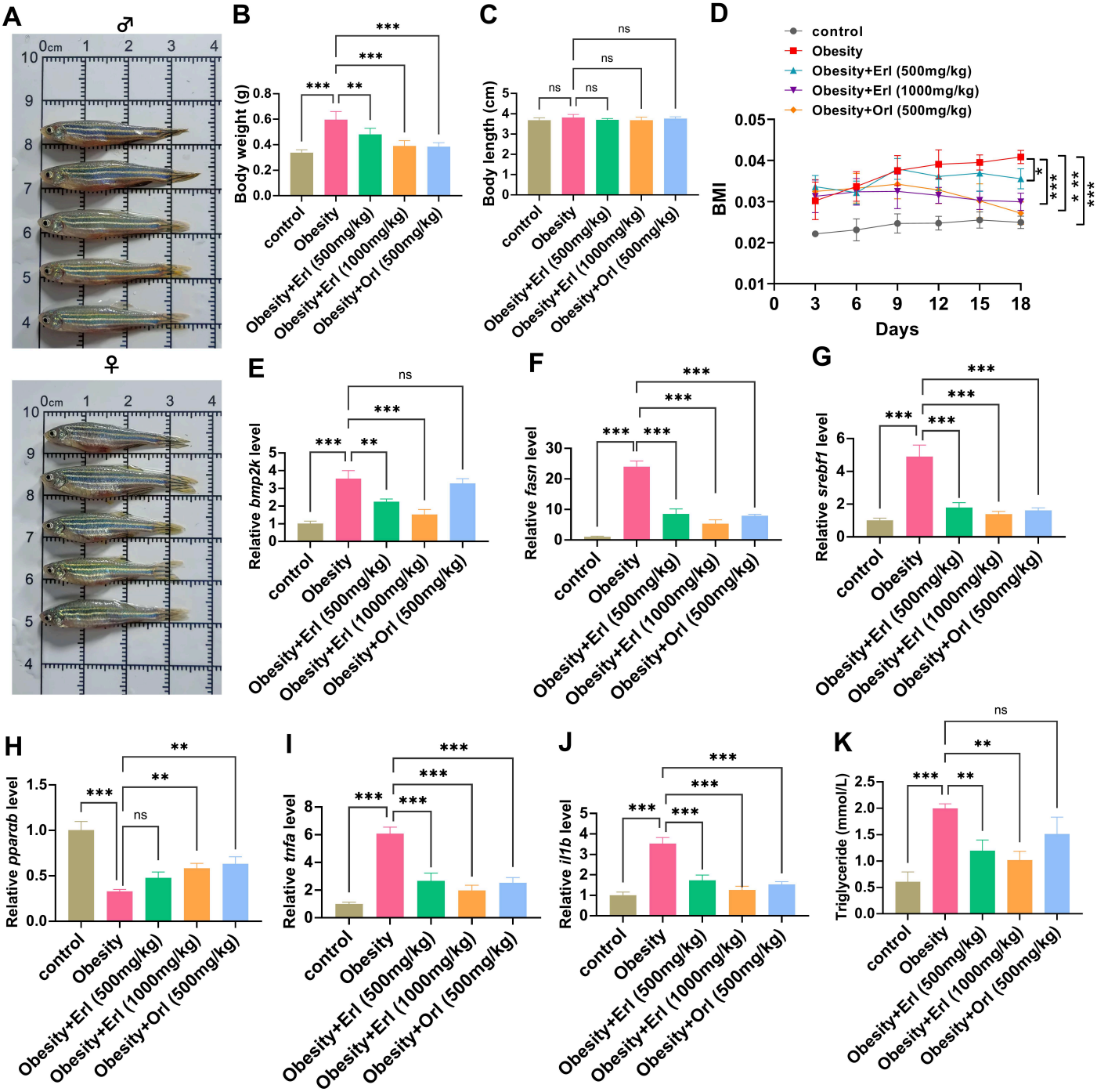


Figure 6

In vivo validation of the anti-obesity effects of Erlotinib in zebrafish.

Representative images showing the external morphology of male and female zebrafish in each experimental group (A). Quantitative analysis of body weight in each group (B). Quantitative analysis of body length in each group (C). BMI analysis of zebrafish in each group (D). Relative expression level of *bmp2k* in each group determined by qRT-PCR (E). Relative expression levels of lipid metabolism–related genes, including *fasn*(F), *srebf1* (G), and *pparab* (H). Relative expression levels of inflammatory cytokines *tnfa* (I) and *il1b* (J). TG levels in each experimental group (K). *P < 0.05, **P < 0.01, P*** < 0.001.

Supplementary Files

This is a list of supplementary files associated with this preprint. Click to download.

- SupTable.xlsx